IVYSPRING INTERNATIONAL PUBLISHER

Theranostics

2017; 7(16): 4013-4028. doi: 10.7150/thno.19304

Research Paper

The Use of PET Imaging for Prognostic Integrin $\alpha_2\beta_1$ Phenotyping to Detect Non-Small Cell Lung Cancer and Monitor Drug Resistance Responses

Chiun-Wei Huang[1], Wen-Chuan Hsieh[1]*, Shih-Ting Hsu[1]*, Yi-Wen Lin[1], Yi-Hsiu Chung[1], Wen-Chi Chang[1], Han Chiu[1], Yun Han Lin[1], Chung-Pu Wu[2, 3, 4, 5], Tzu-Chen Yen[1, 6]✉ and Feng-Ting Huang[7]✉

1. Center for Advanced Molecular Imaging and Translation (CAMIT), Chang Gung Memorial Hospital, Tao-yuan, Taiwan;
2. Graduate Institute of Biomedical Sciences, College of Medicine, Chang Gung University, Tao-Yuan, Taiwan;
3. Department of Physiology and Pharmacology, College of Medicine, Chang Gung University, Tao-Yuan, Taiwan;
4. Molecular Medicine Research Center, College of Medicine, Chang Gung University, Tao-Yuan, Taiwan;
5. Department of Neurosurgery, Chang Gung Memorial Hospital, Tao-Yuan, Taiwan;
6. Department of Nuclear Medicine, Chang Gung Memorial Hospital, Taoyuan, Taiwan;
7. Department of Biochemical Science and Technology, College of Life Science, National Taiwan University, Taipei, Taiwan.

* Wen-Chuan Hsieh and Shih-Ting Hsu contributed equally to this work.

✉ Corresponding authors: Tzu-Chen Yen, M.D. Ph.D., Department of Nuclear Medicine, Chang Gung Memorial Hospital, No. 5, Fu-Hsin St., Kweishan, Taoyuan, 33305 Taiwan Tel.: 886-3-3281200 ext. 2744 Fax: 886-3-211-0052 E-mail: yen1110@cgmh.org.tw Feng-Ting Huang, Ph.D., Department of Biochemical Science and Technology, National Taiwan University, No. 1, Sec. 4, Roosevelt Rd., Taipei 10617, Taiwan Tel.: 886-2-3366-4083 Fax: 886-2-3366-2271 E-mail: fthuang@ntu.edu.tw

Received: 2017.01.23; Accepted: 2017.08.14; Published: 2017.09.20

Abstract

PURPOSE: Growing evidence has demonstrated that aberrant expression of integrin α2β1 might contribute to the invasion, metastasis and drug resistance of non-small cell lung cancer (NSCLC). Thus, the integrin α2β1 targeting ^{68}Ga-DOTA-A2B1 tracer was validated in NSCLC in contrast to accumulation of the clinically used ^{18}F-FDG PET tracer to see if ^{68}Ga-DOTA-A2B1-PET imaging can offer a valuable and critical diagnostic imaging criterion for the identification of phenotypes of aggressive lung cancer.

METHODS: To verify the prognostic value of integrin α2β1, several quantitative and functional *in vitro* assays were validated in different NSCLC cell lines (CL1-0, CL1-5, A549 and selected A549^{++} cells). Positron emission tomography (PET) imaging studies using both standard ^{18}F-FDG and a newly developed ^{68}Ga-labeled integrin α2β1 (^{68}Ga-DOTA-A2B1) tracer were sequentially performed on mice with lung tumor xenografts in different anatomic locations (subcutaneous, orthotopic and osseous) to validate the targeting capability of the ^{68}Ga-DOTA-A2B1 tracers. Treatment responses were monitored by injecting animals with metastatic bone tumors with 5 mg/kg doxorubicin. All *in vivo* treatment responses in each treatment subgroup were monitored with a PET imaging system to evaluate the up-regulation of integrin expression at the earliest stage of treatment (6 h).

RESULTS: The PET and computed tomography (CT) images from NSCLC xenograft animals unambiguously demonstrated accumulation of the integrin tracer ^{68}Ga-DOTA-A2B1 in the tumor lesions at all locations. The average tumor uptake and tumor-to-normal (T/N) ratio were 2.51 ± 0.56 %ID/g and T/N = 2.82, 3.40 ± 0.42 %ID/g and T/N = 1.52, and 1.58 ± 0.108 %ID/g and T/N = 2.31 in subcutaneous, orthotopic and osseous tumors, respectively (n = 5; $p < 0.05$). The xenograft tumors were all clearly visible. In contrast, the accumulation of ^{18}F-FDG reached 3.6 ± 0.76 %ID/g, 1.39 ± 0.075 %ID/g and 3.78 ± 0.73 %ID/g in subcutaneous, orthotopic and osseous tumors, respectively (n = 5; $p < 0.05$). However, due to the high background uptake by normal tissue, the T/N values were less than or close to 1, making the tumors almost indistinguishable in the PET imaging analysis. Furthermore, ^{68}Ga-DOTA-A2B1-PET imaging of the treated osseous tumor model demonstrated more than 19% tracer uptake in A549 lesions (1.72 ± 0.95 %ID/g vs. pretreatment 1.44 ± 0.12 %ID/g,p = 0. 015) 6 h post-treatment with doxorubicin. The elevated intensity of tracer uptake was in accordance with the results of *in vitro*Western blot and *ex vivo* integrin staining, demonstrating elevated integrin α2β1 expression.

CONCLUSION: In this study, integrin α2β1 was identified as a biomarker of aggressive malignant NSCLC. Thus, efforts should be devoted to validating integrin α2β1 as a potential target for non-invasive diagnosis and as a predictive marker for monitoring treatment responses using a preclinical PET imaging system.

Key words: Integrin α2β1, Positron emission tomography, Non-small cell lung cancer, Phenotyping imaging, Treatment response monitoring.

Introduction

Non-small cell lung cancer (NSCLC) is the most common and deadly cancer, despite the reduced risk associated with smoking cessation. The number of NSCLC cases is expected to continually increase because the effect of population aging outweighs the effect of smoking cessation [1] and due to the deleterious air pollution issues in developing countries. Given the inherent heterogeneity of tumors [2], NSCLC treatment is becoming increasingly personalized; thus, the number of patient-tailored therapies has multiplied in recent years [3-7]. Targeted drugs usually cost more than generalized drugs and only benefit a subset of patients, indicating the increasing need to molecularly characterize tumors to select patients for these targeted therapies. Thus far, however, a major hindrance to understanding the stage of lung cancer progression has been the inability to identify a definite marker for tumor diagnosis and staging, thus making patient stratification for specific targeted treatment difficult.

Based on increasing clinical evidence, positron emission tomography (PET) imaging has transformed from a solely diagnostic imaging system to a versatile imaging modality for early tumor lesion detection, therapeutic treatment selection, and recovery and follow-up monitoring in cancer patients [8]. When nuclear PET imaging is combined with other anatomic imaging systems, such as X-ray computed tomography (CT) and magnetic resonance imaging (MRI), profound improvements in the accuracy of disease diagnosis and staging and the development of precise treatment plans for cancer patients are feasible [9, 10]. As elevated glycolytic metabolism is an important hallmark of cancer, the expression levels of hexokinase I and the glucose transporter GLUT1 are up-regulated [11-13]. Thus, the glucose analog ^{18}F-fluorodeoxyglucose (FDG) is the most widely used radiotracer for tumor diagnosis and characterization in clinical settings. However, due to considerable FDG uptake in non-malignant or therapy-induced inflammatory disorders, FDG-PET shows limited specificity for discriminating inflammatory responses from malignancy in the early assessment of treatment responses in patients; this limitation prompted the development of new radiotracers that can be used to specifically visualize and uncover the alternative molecular mechanisms associated with therapy resistance and drug interactions [14, 15].

A variety of integrin αvβ3 targeting-based PET tracers have recently been reported for imaging tumor lesions with high integrin αvβ3 expression *in vivo* and have proceeded to the early phases of clinical trials [16-19]. In addition to integrin αvβ3, integrin α2β1 represents a unique prognostic biomarker, especially for the detection of aggressive or metastatic tumors [20-22]. In particular, the investigation of integrin α2β1 may provide new insights into the molecular events involved in lung carcinogenesis that are controlled by interactions between integrin α2β1 and growth factor signaling cascades, such as extracellular signal-regulated kinase (ERK) and PI3K phosphorylation [23-25]. The integrin α2β1-targeting peptide sequence Asp-Gly-Glu-Ala (D-G-E-A) was previously discovered by Staatz Wd *et al.* [26]. The construct has been further explored and validated in various tumor models for its ability to deliver the desired imaging construct to lesion sites where integrin α2β1 is highly expressed [27-29].

In this study, the prognostic integrin α2β1-targeting PET agent that can target malignant NSCLC and simultaneously monitor the therapeutic intervention response was investigated. Our results suggest that substantial overexpression of integrin α2β1 might serve as an independent prognostic and predictive marker for tumor detection and could be a valuable treatment response monitoring tool for the clinical management of NSCLC with *in vivo* PET imaging.

Materials and Methods

General

All commercially available chemical reagents were of analytic grade and used without further purification. The integrin α2β1 targeting peptide DOTA-Ahx-Cys-Ahx-cyclo[Gly-Asp-Gly-Glu-Ala-D-Tyr-Lys] (^{68}Ga-DOTA-A2B1) (Figure 1) was designed and purchased from Peptides International (Kentucky, US). The $^{68}GaCl_3$ solution was produced by eluting 0.05 N HCl through a ^{68}Ge/^{68}Ga generator (itG, Germany). Purification of the crude product was carried out on an analytical reverse-phase HPLC system equipped with a dual ultraviolet absorbance detector (Waters 2487, Waters, Milford, MA) using a

Phenomenex (Torrance, CA) synergi 4 m Hydro-RP 80A° (150×3×4.6 mm, 4 µm). The flow was 1 mL/min, with the mobile phase starting with 98% solvent A (0.1% trifluoroacetic acid (TFA) in water) and 2% solvent B (0.1% TFA in acetonitrile) (0−2 min) and transitioning to 35% solvent A and 65% solvent B over 30 min.

Cell lines and tumor models

The A549 human lung carcinoma cell line was obtained from the American Type Culture Collection (ATCC; Manassas, VA) and cultured in an incubator with 5% CO_2 at 37 °C. The culture medium was ATCC-formulated F-12K medium (Catalog No. 30-2004) supplemented with 10% fetal bovine serum (FBS) and 1% penicillin-streptomycin. The human lung cancer cell lines CL1-0 and CL1-5 were kind gifts from Dr. Pan-Chyr Yang, National Taiwan University. The CL1-0 cell line was originally established from a 64-year-old man with a poorly differentiated adenocarcinoma, and the CL1-5 cell line is a progressively invasive subpopulation of CL1-0 cells generated through *in vitro* invasion and selection [30]. The cells were maintained in RPMI-1640 supplemented with 10% FBS (Gibco BRL, Gaithersburg, MD).

All animal experiments were performed according to a protocol approved by the Institutional Animal Care and Use Committee (IACUC) of the Laboratory Animal Center, Chang Gung Memorial Hospital, Taiwan. Athymic male nude mice (approximately 6−8 weeks old with body weights of 20−25 g) were obtained from the National Laboratory Animal Center (Taipei, Taiwan) and were housed in groups of five under standard conditions with temperature and light control consisting of a 12 h light/dark cycle and with *ad libitum* access to water and food. During the tumor implantation process, animals were kept in specific pathogen-free conditions and anesthetized with isoflurane gas (2% isoflurane mixed with 100% oxygen). The animals were then returned to a clean cage and kept under warming lamps until complete recovery from anesthesia. For the subcutaneous tumor model, A549 cells (5×10^6) were subcutaneously injected into the front flank region of male athymic nude mice. Tumors were allowed to grow for 3−5 weeks until reaching 200−500 mm^3 in volume. Tumor growth was assessed based on caliper measurements of perpendicular dimensions. The orthotopic lung cancer model was developed similar to the subcutaneous model, but the tumor cells were injected through the tail vein (2×10^6 cells). For the osseous metastasis tumor model, male athymic mice were anesthetized with isoflurane gas (2% isoflurane mixed with 100% oxygen), and an incision was made in the hind limb. Intra-tibial implantation was performed with a 20-µL cell suspension of redshifted firefly luciferase-transfected A549 tumor cells (1.5×10^6). Tumor growth was followed up with weekly bioluminescence imaging. Treatment response monitoring experiments were performed by injecting metastatic bone tumor animals with 5 mg/kg doxorubicin. All *in vivo* treatment responses from the treatment subgroups were monitored using a PET imaging system to evaluate the up-regulation of integrin expression levels at the earliest stage of treatment (6 h). To keep animal welfare considerations in mind, severely inert mice and mice carrying unusually large tumors (outliers) were euthanized and removed from the experiment to avoid or alleviate unnecessary suffering or distress.

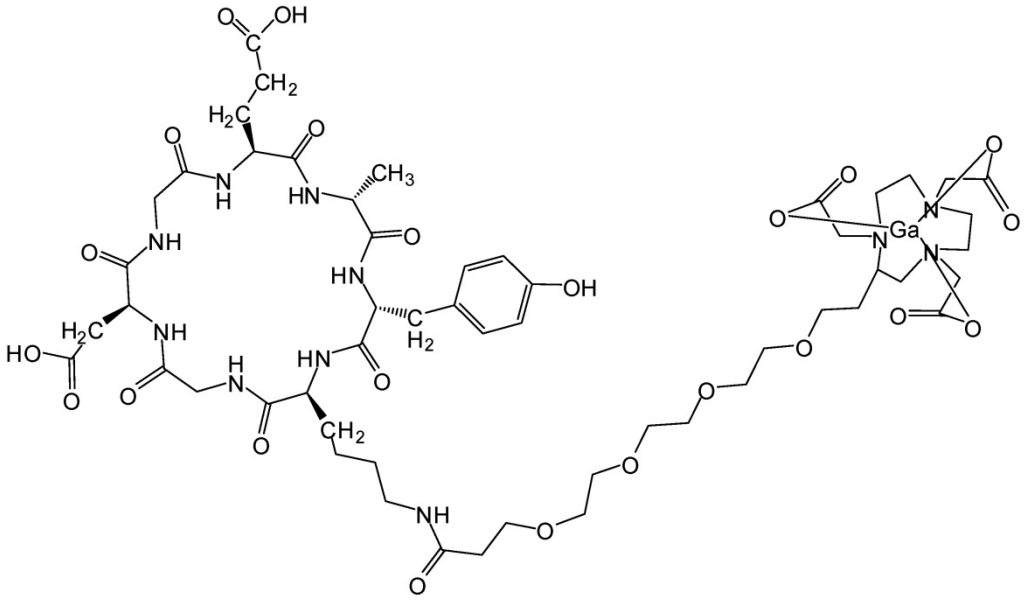

Figure 1. Integrin α2β1 targeting peptide tracer. The chemical structure of ^{68}Ga-DOTA-Ahx-Cys-Ahx-cyclo [Gly-Asp-Gly-Glu-Ala-D-Tyr-Lys].

Western blot

Each lung cancer cell line (A549, CL1-5, and CL1-0) was homogenized with lysis buffer containing protease inhibitors. Then, 20 μg of total protein was resolved by 10% SDS-PAGE and transferred to polyvinylidene difluoride membranes, blocked, and incubated with α-integrin α2 (1:10,000; ab133557, Abcam), α-integrin β1 (1:10,000; GTX128839, Gene-Tex), or α-tubulin (T6074, Sigma) antibody. After washing, the membrane was incubated with HRP-conjugated goat α-rabbit secondary antibody (1:10,000), followed by the addition of Immobilon Western Chemiluminescent HRP Substrate (Millipore, MA) and measurements made using a BioSpectrum imaging system (UVP).

Flow cytometry analysis and sorting

First, 1×10^6 A549 cells were incubated with mouse α-integrin α2β1 antibody (ab24697, Abcam) on ice for 30 min, followed by incubation with FITC goat α-mouse antibody (554001, BD) on ice for another 30 min. The samples were then washed three times and re-suspended in phosphate-buffered saline (PBS). The stained samples were analyzed using a BD FACSCanto II, and data were collected from 1×10^4 viable cells. Experimental data were analyzed with Flowjo7.2.2 software. For FACS sorting of cells with high expression levels of integrin α2β1, only the top 25% of the integrin α2β1-overexpressing cancer cells were collected and expanded for second-round selection. The subline from the first round of selection was designated $A549^{+}$, and the subline from the second round of selection was designated $A549^{++}$. The proliferation of A549, $A549^{+}$ and $A549^{++}$ cells was validated with a CCK8 assay, which indicated no significant difference among these cell lines (p = 0.1; Figure S1).

In vitro migration assay

Culture inserts (Ibidi, Germany) were placed in a 24-well plate, and 2×10^4 A549 cells were seeded per chamber. After incubation for 28 h, the insert was removed, and cells were stained with 1 μg/mL Hoechst 33342. Cell migration was monitored continually in real-time using an IN Cell Analyzer 2000 (GE Healthcare Life Sciences) for 28 h and analyzed with the IN Cell Developer Toolbox. The number of cells migrating into the gap was calculated and analyzed.

In vitro invasion assay

8 μm transwell inserts (Millicell® Hanging Cell Culture Insert) were used to measure cell line invasion capabilities. First, diluted Matrigel was coated on the inserts in a 24-well plate. Subsequently, 100 μL of cell suspension (4×10^4 A549 cells in serum-free RPMI medium) was seeded onto the insert. Then, 600 μL RPMI containing 1% FBS was added to the lower well. After 20 h, the cells below the insert were fixed with 95% methanol and stained with 0.2% crystal violet in methanol. Cells above the insert were removed with cotton swabs. The invaded cells were microscopically counted, and the numbers of cells from three different fields of view were averaged.

Experimental metastasis

The NSCLC cell lines CL1-0, CL1-5, and A549 and the high integrin α2β1-expressing $A549^{++}$ cells were trypsinized and re-suspended in PBS. Subsequently, a single-cell suspension containing 1×10^6 cells in 0.1 ml PBS buffer was injected into the lateral tail vein of 4- to 6-week-old BALB/c nude mice. The mice were sacrificed after 8 weeks. All organs were examined for metastasis formation. The lungs were removed and embedded in OCT, and the tissue was then sectioned into 20 μm layers and stained with hematoxylin and eosin (H&E) for histological analysis. The number of lung tumor colonies was counted under a dissecting microscope.

Radiochemistry

The metal chelator 1,4,7,10-tetraazacyclododecane-1,4,7,10-tetraacetic acid (also known as DOTA) was chosen to conjugate the targeting peptide construct and was labeled with ^{68}Ga radio-metal ions for PET image acquisition. In brief, the eluted $^{68}GaCl_3$ was added to a DOTA-conjugated peptide agent in 0.1 M sodium acetate (pH 5.5) and incubated at 95 °C for 5 min. Due to the high labeling yield, the ^{68}Ga-labeled peptide tracer could be directly used without further purification. The radiochemical purity of the final products (^{68}Ga labeled tracers) was confirmed by radio-HPLC. The HPLC-verified products were then reconstituted in PBS to 1 mCi/mL and passed through a 0.22 μm Millipore filter into a sterile multi-dose vial for *in vitro* and *in vivo* imaging experiments.

Receptor binding assay

The α2β1 receptor-binding affinity of the radiolabeled ^{68}Ga-DOTA-A2B1 peptide tracer was evaluated using CL1-5 and A549 cancer cells (α2β1 integrin-positive). Briefly, the assay was performed by incubating 2×10^5 A549 cells with ^{68}Ga-DOTA-A2B1 peptides (~150 kBq) and varying concentrations of non-radiolabeled A2B1 peptides in binding buffer [IBB, 25 mM Tris pH 7.4, 150 mM NaCl, 2 mM $CaCl_2$, 1 mM $MgCl_2$, 1 mM $MnCl_2$, and 0.1% bovine serum albumin (BSA)] at room temperature for 1 h. The

varying amounts of integrin α2β1-targeting peptide were expected to inhibit the binding of the radio-tracer to tumor cells in a concentration-dependent manner. The cell-bound radioactivity that remained after washing three times with PBS containing 0.1% BSA was determined by gamma counting. The best-fit 50% inhibitory concentration (IC_{50}) values were calculated by fitting the data with nonlinear regression using GraphPad Prism. Each data point represents the result calculated from triplicate wells.

Cell uptake and efflux studies

Cell uptake and efflux studies were performed to quantify the internalization levels of the peptides. Experiments were performed with triplicate wells. A549 and CL1-5 cells (7×10^4) were plated into 24-well plates overnight before ^{68}Ga-DOTA-A2B1 uptake analysis. On the day of the experiment, fresh, pre-warmed RPMI-1640 containing 150 KBq of ^{68}Ga-DOTA-A2B1 was added to individual wells. Cells were incubated with ^{68}Ga-DOTA-A2B1 at 37 °C and 5% CO_2 over a 90 min time course. At the indicated time points (5 min, 15 min, 30 min, 60 min and 90 min), cells were rinsed two times with ice-cold PBS and lysed with NaOH-sodium dodecyl sulfate (SDS) (0.2 M NaOH, 1% SDS). The cell lysate was collected in counting tubes, and decay-corrected radioactivity was measured on a gamma counter (Cobra II Auto-Gamma Counter; Packard Biosciences Co.). The cell uptake was quantified by standards from the solution (300 KBq/ml) added to cells into percentage of radiotracer uptake. For efflux studies, cells were incubated with radio-tracer for 90 min and washed two times with room temperature PBS solution before subsequent incubation at 37 °C in fresh, radiotracer-free and serum-free RPMI medium. At the specified times, samples were processed as described above.

In vitro integrin tracer stability assay

The *in vitro* stability of ^{68}Ga-DOTA-A2B1 in PBS was also determined by measuring the radiochemical purity at different time points at 37 °C. Samples of the resulting solutions were analyzed by radio-HPLC at 0 min, 30 min, 60 min, and 90 min after extraction. The *in vitro* stability in serum was also examined. ~3.7 MBq of ^{68}Ga-DOTA-A2B1 in 50 μL of PBS was added to 450 μL of mouse serum and incubated at 37 °C. ~50 μL of this serum sample was removed at 0 min, 30 min, 60 min, and 90 min and placed in a plastic tube. An equal volume of acetonitrile was added to each tube, which was then centrifuged at 6,000 rpm for 10 min. The supernatant was separated from the pellet, and the supernatant was diluted with 300 μL water and injected into an analytical radio-HPLC.

Small-animal PET imaging of tumors

Groups (n = 5) of athymic male nude mice bearing subcutaneous, orthotopic or osseous A549 tumor xenografts were intravenously (i.v.) administered ~7.4 MBq of ^{68}Ga-DOTA-A2B1 tracer, and sequential PET/CT scans were acquired at 10 min post-injection (p.i.). This time point was selected considering the physical half-life of ^{68}Ga (68 min) and the typical short circulation times of peptide tracers (~10 min). Also, the best imaging contrast during this time frame was confirmed by the 60 min dynamic PET scanning and time-activity curves of major organs and the tumor. The FDG-PET (~11.1 MBq; 60 min p.i.) scans were also conducted in tumor-bearing mice (fasted overnight and kept under isoflurane anesthesia during the uptake and imaging acquisition periods to reduce the non-specific background uptake) for comparison studies. PET/CT studies were performed on an Inveon microPET rodent model scanner (Siemens Medical Solutions USA, Inc.). Anesthesia was induced with 4% isoflurane and maintained at 2%, and the mice were placed near the center of the field of view, where the highest resolution and sensitivity values were obtained. In addition, blocking studies were performed to validate the targeting specificity by co-injecting an unlabeled integrin α2β1 targeting c(DGEAyK) peptide (10 mg/kg body weight) with the ^{68}Ga-DOTA-A2B1 tracer through the tail vein (n = 3).

To improve image quality, 20 million coincidence events per mouse were acquired for each static PET emission scan (energy window, 350−650 keV; time window, 3.432 ns; resolution, 1.5 mm). All mice received CT imaging for anatomic registration following PET imaging. The reconstructed images had a matrix size of 128×128×159 mm with 0.14×0.14×0.14 mm using the 2D ordered-subset expectation maximum iterative method. All images were carried out with scatter correction, random correction and attenuation correction (AC). AC was carried out by transmission scans with ^{68}Ge/^{68}Ga and a rotating line source. The quantitative regions of interest (ROIs) of the tumors or organs are presented as the percent injected dose per gram (%ID/g) in the coronal plane using PMOD version 3.2 image analysis software (PMOD Technologies Ltd., Zurich, Switzerland). The tumor to normal tissue (T/N) radioactivity ratio was also calculated for comparison. To assess the complete distribution profile of the tracer, A549 tumor-bearing mice were sacrificed after the image scans. Selected organs were excised and weighed, and the radioactivity was counted with an automatic γ–counter (Perkin-Elmer). The

biodistribution data are presented as the percentage of the injected dose per gram (%ID/g; mean ± SD).

Autoradiography and immunohistochemistry studies

After performing *in vivo* PET imaging studies, A549 lung tumors were excised and embedded in OCT compound (Tissue-Tek), snap-frozen in a dry ice-filled chamber, and then cryosectioned with a thickness of 20 μm. Autoradiographs were collected using a Cyclone Pulse Storage Phosphor system (Perkin-Elmer, USA) with an exposure time of 24 h. The white-light images of these lung sections were taken with a Leica MZ75 (Leica Inc., Germany) high-performance stereomicroscope equipped with a 2.5x Plano objective. To histologically investigate the expression level of integrin receptors, immunohistochemistry was used to confirm the co-localization of activated integrin and the accumulation of the imaging agent in autoradiography results. The resulting tumor histological slides were fixed in methanol, dehydrated, and pre-incubated with 0.3% H_2O_2 to block endogenous peroxidase activity. The sections from tumors were blocked with 1% BSA for 1 h and then incubated with α-integrin α2β1 monoclonal antibodies (ab24697, dilution 1:50 in Tris buffer) at 4 °C overnight. After washing with TBS, the slides were incubated with HRP-conjugated goat α-mouse IgG secondary antibody (dilution 1:200 in Tris buffer) for 1 h at room temperature. The reaction was developed in 3, 3'-diaminobenzidine (Sigma).

Statistical analyses

Quantitative data were analyzed using unpaired, 2-tailed Student's *t*-tests, and the results are expressed as the mean ± SD. Differences at the 95% confidence level ($p < 0.05$) were considered to be statistically significant. All groups included a minimum of three subjects ($n \geq 3$).

Results

Integrin α2β1 expression is associated with an aggressive NSCLC phenotype

The ectopic overexpression of integrin α2β1 is thought to bestow untransformed cells with both tumorigenic and metastatic potential in various malignant cancers [31-36]. Moreover, the up-regulation of integrin α2β1 has been associated with increased radio-resistance and chemo-resistance in tumors [24, 25]. Thus, we first evaluated the expression level of integrin α2β1 in several NSCLC cell lines (CL1-0, CL1-5 and A549) at the protein level by Western blot and at the cell surface distribution level by flow cytometry. CL1-0 is a human lung adenocarcinoma clonal cell line established from a lung cancer patient, and CL1-5 is an aggressive subtype of CL1-0 isolated through transwell invasion screening and single-colony selection [30]. According to the Western blot results (Figure 2A), the relative levels of integrin α2 and β1 proteins were found to be significantly higher in the advanced NSCLC carcinoma cell lines CL1-5 and A549 than in the matched control cell line CL1-0 ($p < 0.05$). The flow cytometry results of the integrin α2β1 distribution were consistent with the Western blot results (Figure 2B). The aggressive A549 and CL1-5 cell lines both demonstrated higher positive staining percentages (97.1% and 95.2%, respectively) than the CL1-0 cell line (14.5%). These results indicate that the enhanced expression of integrin α2β1 seems to be associated with the invasive behavior of lung tumor cells.

To further validate this hypothesis, the ATCC A549 cell line was chosen for migration and invasion assays and *in vivo* metastatic potential studies to confirm that the aggressive phenotype was due to the effect of integrin α2β1 rather than the intrinsic properties of the different cell lines. Thus, the subpopulation with high integrin α2β1 expression was sequentially enriched by cell sorting followed by single-cell clone selection (Figure S1). The parental A549 cells and the selected integrin α2β1-enriched A549 cells were defined as the A549 and A549^{++} groups, respectively. The migration assay demonstrated that A549^{++} cells filled the migration gap 3.65-fold faster than the parental A549 cells (84% vs. 23%, $p < 0.05$) (Figure 2C). Additionally, the invasion capability of A549^{++} cells was 2.48-fold higher than that of the parental A549 cells in the Matrigel-coated transwell assay (87% vs. 35%, $p < 0.05$). Furthermore, the *in vivo* experimental metastasis study revealed that A549^{++} cells also demonstrated a high potential for producing lung metastasis 8 weeks after tail vein injection of the cells (5/5), whereas only 3/5 mice injected with A549 cells showed distinct lung tumor colonies (Table 1). Collectively, our results suggest that the high integrin α2β1 expression in A549 cells led to enhanced tumor cell migration, invasion and metastatic potential, which are typical features of tumor malignancy. These findings indicate that integrin α2β1 could serve as a potential clinically valuable biomarker for identifying NSCLC with an aggressive phenotype.

Integrin α2β1-targeting DGEAyK peptide derivatives have been identified and validated in various tumor models to have the ability to deliver the desired imaging construct to lesion sites where integrin α2β1 is highly expressed [27-29]. The DOTA chelator-based ^{68}Ga radiolabeling strategy was chosen based on its simple synthesis, high labeling efficiency

and lower radio-burden due to the short half-life of the ^{68}Ga isotope ($t_{1/2}$ of 68 min). The peptide tracer ^{68}Ga-DOTA-A2B1 construct (Figure 1) can be divided into three components: 1) a cyclized peptide scaffold with the integrin α2β1-targeting sequence (cyclo [Gly-Asp-Gly-Glu-Ala-D-Tyr-Lys]), 2) a conjugated linker structure (-Ahx-Cys-Ahx-), and 3) bifunctional DOTA chelators incorporated into the imaging agent structure for radiolabeling. The radiolabeling of DOTA-A2B1 with ^{68}Ga was accomplished with a high yield (95%), radiochemical purity (> 98%), and specific activity (~27.7 GBq/mg), and quality-control assessments of ^{68}Ga-labeled tracers were performed according to the European Pharmacopoeia 8 (Table S1). An *in vitro* competitive cell-binding assay was used to determine the receptor-binding affinity of ^{68}Ga-DOTA-A2B1. The non-radiolabeled A2B1 peptide was used as the competitor in this assay. The cold A2B1 peptides inhibited the binding of ^{68}Ga-DOTA-A2B1 to α2β1 integrin-positive CL1-5 and A549 cells in a dose-dependent manner, and the IC_{50} values for inhibition were calculated as 4.23 ± 0.25 μM and 3.72 ± 0.21 μM (n = 3) in CL1-5 and A549 cells, respectively (Figure 3).

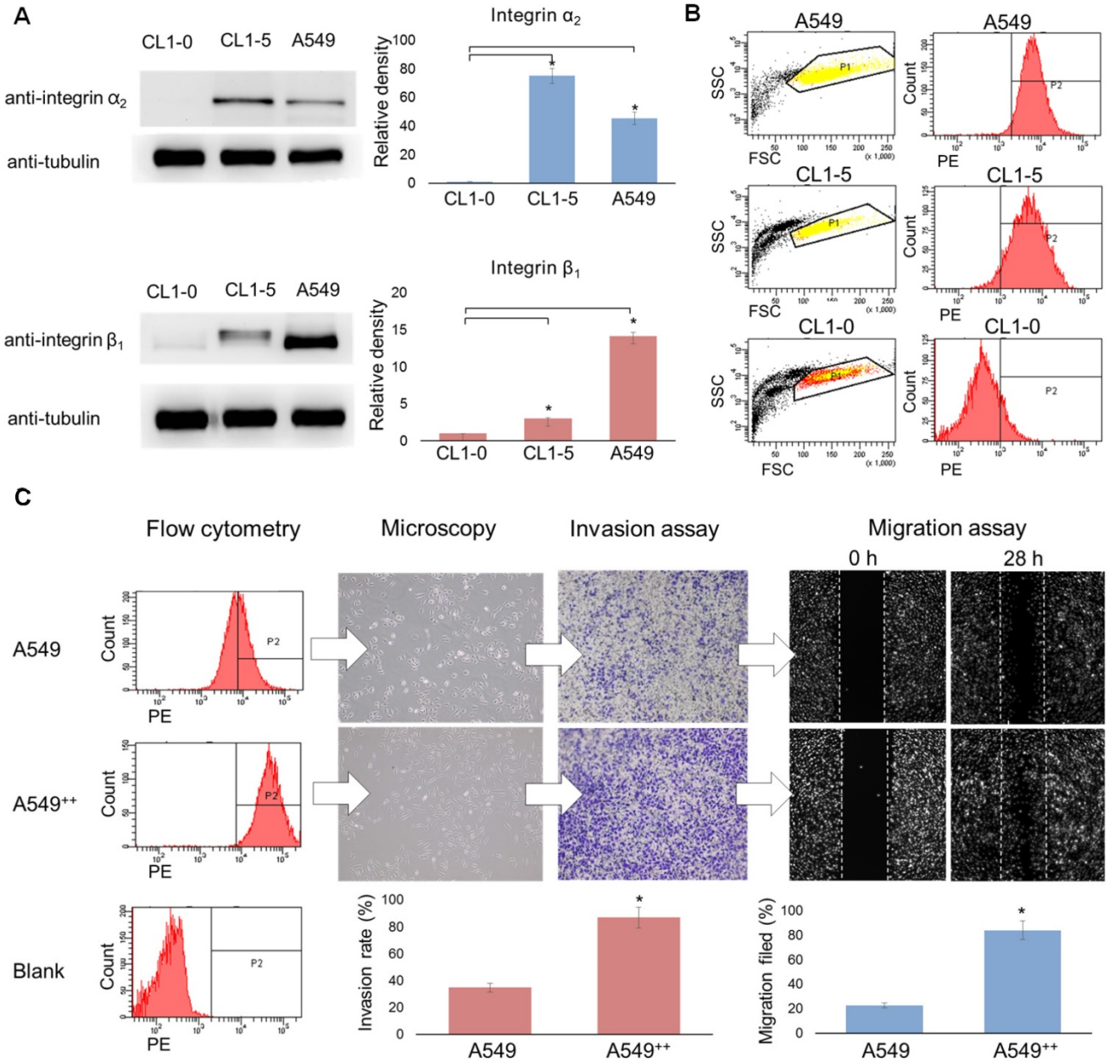

Figure 2. Over-expression of integrin α2β1 is associated with the malignant phenotype of human non-small cell lung cancer. (A) Western blot analysis of integrin α2 or β1 expression in the lung cancer cell lines CL1-0, CL1-5 and A549. (B) Flow cytometry was performed to evaluate the distribution level of integrin α2β1 on the tumor surface. (C) Using cell sorting, A549 cells were separated into two populations, non-sorted A549 and integrin α2β1-high A549^{++} cells, and the correlations between the integrin α2β1 level and the association with migration and invasion capabilities were determined. The A549^{++} population displayed a marked expression signature corresponding to a more aggressive NSCLC phenotype. Error bars represent the standard deviation of the mean. *$p < 0.05$.

Table 1. Number of BALB/c nude mice found with lung tumor nodules 8 weeks following injection with tumor cells. Experimental lung metastasis of cell-line variants selected from FACS sorting.

Cell lines	Number of Cells Injected/mouse	Number of Tumors in each injected/mouse[1]
CL1-0	10^6	0/5
CL1-5	10^6	2/5
A549	10^6	3/5
$A549^{++}$	10^6	5/5

[1] Number of mice with tumors: number of mice with tumors/total number of injected mice.

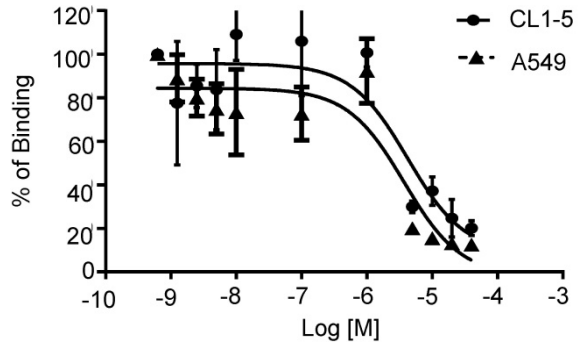

Figure 3. *In vitro* inhibition of ^{68}Ga-DOTA-A2B1 binding to integrin α2β1 on CL1-5 and A549 cells by varying amounts of A2B1 peptides (n = 3, mean ± SD).

The cell uptake and efflux assay results demonstrated uptake and efflux profiles that were similar to those of other integrin tracers. In brief, due to the low binding affinity of the integrin tracer, the ^{68}Ga-DOTA-A2B1 uptake rates of these two cell lines were below 1%, which is similar to previously reported monomeric integrin tracers, such as RGD peptides (Figure 4). In addition, the two cell lines showed rapid and substantial efflux when the labeled cells were cultured in serum-free medium, implying that radioligands may only bind to the cell-surface without internalization.

The serum stability of the ^{68}Ga-DOTA-A2B1 tracers was also evaluated by incubation in mouse serum (90% serum: 10% PBS) at 37 °C for 1.5 h, and 87 % radioactivity was found in the supernatant after treatment with acetonitrile extraction. The recovery percentage of intact peptide probes was over 90 %, as verified by the radio-HPLC profile (Figure S2).

In vivo integrin α2β1 PET imaging in a subcutaneous tumor model

High expression levels of integrin α2β1 were found to be correlated with tumorigenic potential among selected lung cancer cell lines (A549 = CL1-5 > CL1-0) in *in vitro* functional assays and *in vivo* experimental metastasis studies, justifying the role of α2β1 as a potential biomarker for malignant lung cancer. To prospectively verify the prognostic value of integrin α2β *in vivo*, integrin α2β1-targeting ^{68}Ga-DOTA-A2B1-PET imaging was compared in parallel with ^{18}F-FDG-PET scans in subcutaneous A549 and CL1-5 xenografts in terms of their metabolic stability and tumor site targeting efficacy. Also, the best imaging contrast of ^{68}Ga-DOTA-A2B1was confirmed by the 60 min dynamic PET scanning and time-activity curves of major organs and the tumor (Figure S3). As early as 10 min after the i.v. administration (7-8 MBq) of the ^{68}Ga-DOTA-A2B1 tracers, the PET images revealed high-contrast signals in xenograft tumors due to the high integrin α2β1 expression levels of xenografts and the rapid clearance of the tracer from non-targeted normal organs and tissues (Figure 5). In A549 and CL1-5 malignancies, 2.51 ± 0.56 %ID/g (n = 5) and 2.15 ± 0.35 %ID/g (n = 5), respectively, of the ^{68}Ga-DOTA-A2B1 tracer was taken up. The T/N (N: normal muscle) ratio of the A549 group and the CL1-5 group was calculated as 2.82 ± 0.76 and 2.75 ±1, making the tumors clearly visible. In contrast, there was greater accumulation of ^{18}F-FDG in the tumor, and the uptake reached 3.6 ± 0.76 % ID/g (n = 5). However, due to the high background uptake (muscle: 3.11 ± 1.05 % ID/g), the T/N value was only 1.15, making the tumors nearly indistinguishable in PET images. These results suggested that there is significantly higher imaging

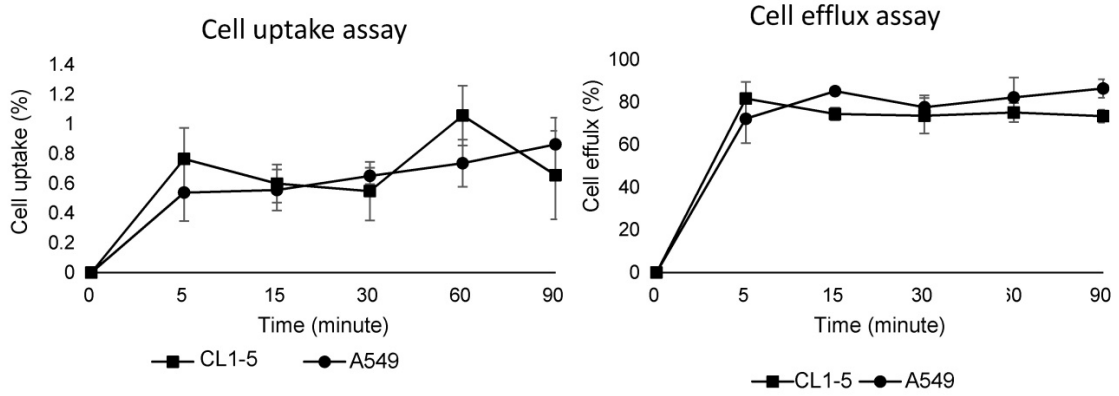

Figure 4. Cell uptake assay (left) and cell efflux assay (right) of ^{68}Ga-DOTA-A2B1 on CL1-5 and A549 cells (n = 3, means ± SD).

contrast using ^{68}Ga-DOTA-A2B1 accumulation than using the clinical ^{18}F-FDG PET tracer, and the high contrast value of ^{68}Ga-DOTA-A2B1 may offer a critical benefit in diagnostic imaging for identifying aggressive NSCLC. Furthermore, the integrin α2β1 receptor specificity of ^{68}Ga-DOTA-A2B1 was confirmed by blocking experiments in which the tracers were co-injected with the c(DGEAyK) peptide (10 mg/kg). As shown in Figure 5, in these experiments, the A549 tumors showed significantly less tracer uptake, with a reduced uptake value of 0.94 ± 0.44 %ID/g ($p < 0.001$) at 10 min after injection. In addition to the lower tumor uptake in the blocking animal model, the distribution of radioactivity in major organs such as the kidneys, liver, muscle, brain, and heart were 7.58 ± 3.56 %ID/g, 3.54 ± 2.1 %ID/g, 0.84 ± 0.49 %ID/g, 0.43 ± 0.21 %ID/g, and 1.62 ± 1.3 %ID/g, respectively, and the kinetics of elimination from circulation were comparable to those in the non-blocked model, which mainly occurred via the renal pathway. Thus, the non-invasive detection of integrin α2β1 activity *in vivo* may serve as a valuable biomarker for overcoming the false-positive (negative) results of FDG-PET scans by using a tracer with more specific uptake. The animals were sacrificed at the end of the scans. The tumors and major organs were dissected, and immunohistochemistry images were acquired to confirm the integrin expression level (Figure S4). The biodistribution data (Figure S5) from direct tissue sampling are expressed as a percentage of the injected dose/gram of tissue (% ID/g) and the ratio of tumor to major organs, and the results were consistent with the PET imaging quantification data (Figure 5B), confirming the binding specificity and favorable biodistribution pattern of integrin tracers.

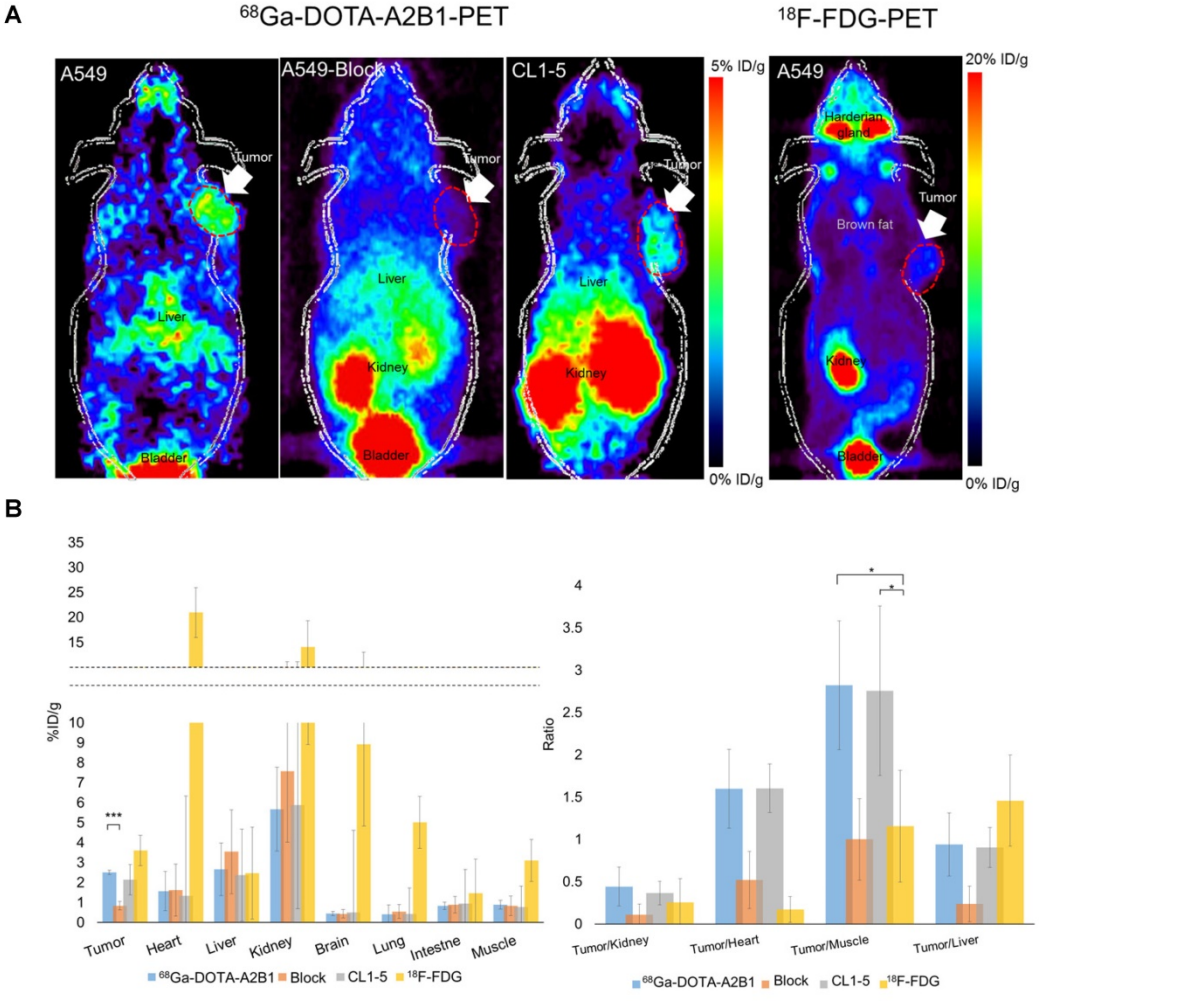

Figure 5. Non-invasive PET imaging of ^{68}Ga-DOTA-A2B1 with/without a blocking dose of c(DGEAyK) peptide and ^{18}F-FDG in integrin α2β1-positive A549 and CL1-5 xenograft mouse models. (A) Decay-corrected whole-body planar coronal PET images of the A549 (or CL1-5) tumor-bearing animal model at 10 min post-injection of 7-8 MBq of ^{68}Ga-DOTA-A2B1 or 11.1 MBq^{18}F-FDG tracer (p.i. 60 min). The blocking group was injected with a high dose of the non-radiolabeled c(DGEAyK) peptide (10 mg/kg), and all images are coronal views. The tumors are indicated with arrows. (B) Region of interest (ROI) analysis of the PET images showing ^{68}Ga-DOTA-A2B1 and ^{18}F-FDG uptake values in the tumor and major organs, such as the heart, lung, kidneys, liver and muscle; values are presented as the % ID/g ± SD (n = 5). The quantified PET imaging data (Figure 5B) indicated the binding specificity and favorable biodistribution pattern of integrin tracers. The tumor/muscle ratios of the ^{68}Ga-DOTA-A2B1 A549 (n = 5) and CL1-5 (n = 5) groups were significantly better (*p) than that of the ^{18}F-FDG group (n = 5), in which the A549 tumor was barely visible ($p < 0.05$). High integrin tracer retention occurred in the urogenital tract due to predominant renal clearance, and intermediate uptake was found in the liver. *$p < 0.05$; *** $p < 0.001$.

Validation of an orthotopic lung cancer model

Despite the success of this proof-of-principle PET imaging study in subcutaneous xenograft models, there remain barriers to the full characterization of the integrin α2β1 targeting tracer *in vivo* and to the eventual clinical translation of such a targeting agent. The major drawback of the subcutaneous lung tumor model is that the xenografts were not placed in the organ environment in which the tumor grows, so cross-talk between the tumor and its microenvironment cannot be preserved or modulated. Therefore, an orthotopic lung tumor model was developed using tail vein injection with A549 lung tumor cells; this model serves as a more clinically relevant animal model for translational purposes.

The PET imaging results of established orthotopic A549 NSCLC tumors unambiguously enabled the acquisition of high-contrast PET signals in small tumor nodules (~2 mm) (Figure 6A). The average tumor uptake was measured as 3.40 ± 0.42 %ID/g, and the T/N (N: normal lung tissue) ratio was 1.52. However, the ^{18}F-FDG tracer did not correspond to a sufficient signal (1.39 ± 0.075 %ID/g; T/N = 0.74) for tumor delineation in the same orthotopic tumor model. Major organ ROI analysis was performed (Figure S6), and *ex vivo* autoradiography was also performed to compensate for the resolution limitation of *in vivo* PET results. Microscopic autoradiography images of excised mouse lung sections showed that integrin tracers penetrated the lung capillaries and could be detected in the tumor nodules (Figure 6B), whereas no detectable (or low) parenchymal delivery of radiolabeled tracers was found. Autoradiography confirmed that the α2β1 radiotracer was specifically present throughout the tumor lesions, and the highest counts were observed within the larger nodules. The calculated autoradiography T/N ratio in the excised lung tumor tissue reached 4.59, which was much greater than that of the FDG tracer control (T/N = 2.57) (Figure S7). Likewise, co-localization analysis indicated excellent positioning accuracy between the autoradiography and immunohistochemical images (> 95%), validating the tracer uptake against *in situ* integrin α2β1 expression (Figure 6B).

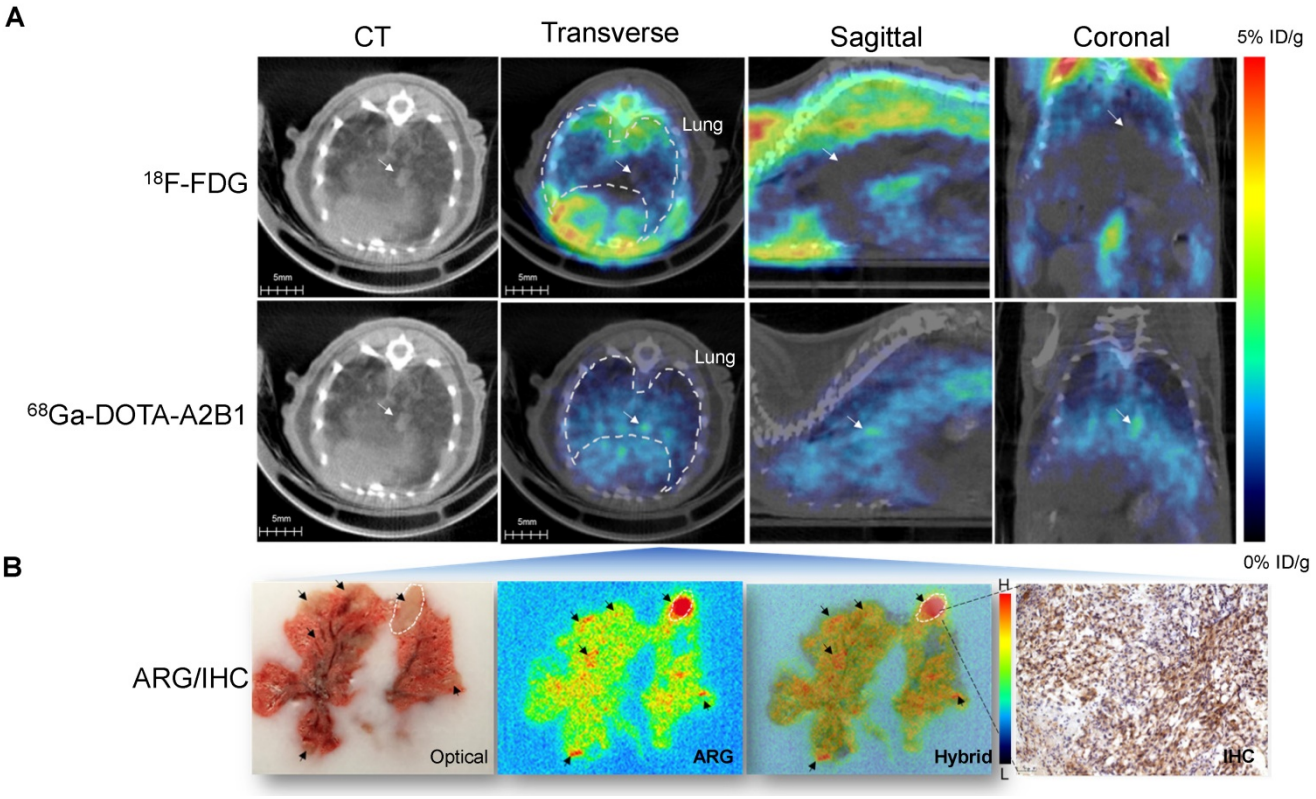

Figure 6. *In vivo* PET/CT imaging and high-resolution autoradiography in the orthotopic lung cancer model after injection of integrin α2β1 tracers. (A) Representative PET/CT imaging of lungs after injection of ^{68}Ga-DOTA-A2B1 and control ^{18}F-FDG. The anatomic drawing based on an image of a mouse lung obtained by a CT scan clearly demonstrates the location of the lung. (B) A digital photograph of a mouse lung embedded in OCT. The arrows indicate the tumor lesions. Autoradiography images acquired from 20-μm tissue slices 15 min after injection of the integrin α2β1 radiotracer. The intratumoral delivery of tracers was evident based on the high radioactivity (displayed as a red color) detected in the tumor nodule areas and as shown in the hybrid image with the photograph. Additionally, immunohistochemistry analysis showed that integrin α2β1 expression was correlated with ARG imaging. The markedly stronger α-integrin α2 staining was observed to be co-localized in tumor nodules with high radioactivity.

Detection of bone metastasis and treatment response monitoring

Distant metastasis is the leading cause of cancer-related deaths, and these metastatic lesions usually show phenotypes that are different from those of the primary tumor, highlighting the importance of disease assessment in this group of patients. PET imaging facilitates selection of the optimal therapy because it can be used for the biological characterization of metastatic lesions at an early time point. Integrin α2β1 is the primary receptor for type I collagen, an abundant protein in skeletal tissues, and elevated integrin α2β1 expression has been shown to result in chemotherapeutic resistance in many cancers [24, 37-40]. We sought to determine the effect of doxorubicin treatment in a bone metastasis model using selected A549^{++} cells. Drug-induced up-regulation of integrin α2β1 protein expression in this cell line was first confirmed by immunoblotting and flow cytometric analysis (Figure 7). In line with previous reports [25, 28, 29, 36-38, 41], elevated integrin α2β1 expression might render A549 cells more resistant to doxorubicin treatment through the MAPK/ERK survival pathway. Based on these *in vitro* studies, we postulated that the drug resistance response in A549 lung cancer cells could be monitored by non-invasive ^{68}Ga-DOTA-A2B1-PET imaging. Thus, skeletal tumors were established in intact male mice through the injection of A549 cells into the tibia of the left (or right) hind limb, and tumor development was longitudinally monitored by IVIS spectrum imaging once per week.

Following doxorubicin treatment (5 mg/kg), the osseous tumor lesions showed specific uptake of ^{68}Ga-DOTA-A2B1 in the implanted tibia (Figure 8A) compared with the contralateral limb (1.44 ± 0.08 %ID/g vs. 0.63 ± 0.057 %ID/g, respectively, $p < 0.05$), and the T/N (N: thigh muscle) ratio reached 2.30 ± 0.17. Furthermore, PET/CT imaging demonstrated significantly higher uptake in A549 lesions (1.72 ± 0.92 %ID/g, $p = 0.015$) as early as 6 h post-treatment with doxorubicin, indicating more than 19 % increased tracer uptake (Figure 8C). The intensity of tracer uptake matched the integrin-staining histochemical results, delineating the elevated integrin expression level (Figure 8D) and justifying that the dynamic phenotype of up-regulated integrin α2β1 can be detected and quantified with ^{68}Ga-DOTA-A2B1-PET imaging. Although ^{18}F-FDG-PET imaging demonstrated high tracer uptake (3.78 ± 0.73 %ID/g), non-specific high thigh muscle (1.65 ± 0.29 %ID/g) or bone ^{18}F-FDG uptake (2.37 ± 0.53 %ID/g) interfered with the quantification of bone metastases in the vicinity of these tissues (Figure 9).

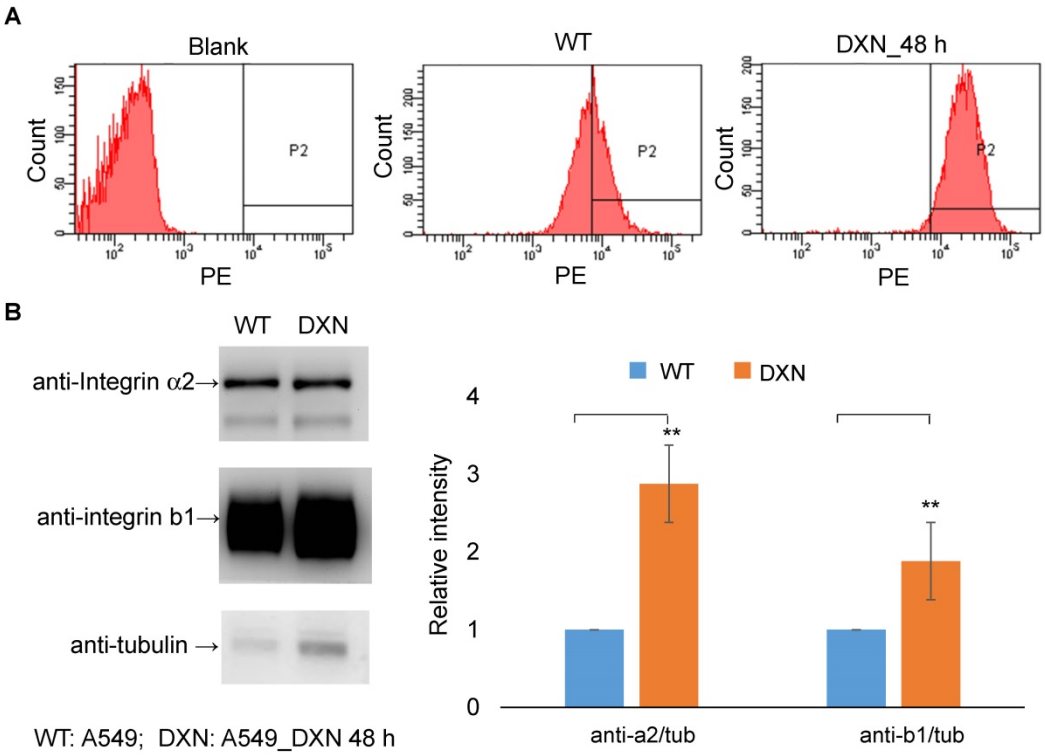

Figure 7. Integrin α2β1 is up-regulated after doxorubicin treatment. (A) *In vitro* FACS analysis of integrin α2β1 expression in wild-type A549 cells (WT) and after doxorubicin treatment (4 μg/mL; 48 h) in A549 cells (DXN). A clear shift in the abundance of integrin α2β1 was observed in the DXN group. (B) Doxorubicin treatment affected the protein levels of integrin α2 and β1 in A549 cells. Semi-quantitative analysis of the Western blot results revealed a markedly higher level of both integrin proteins in DXN cells (**$p < 0.01$).

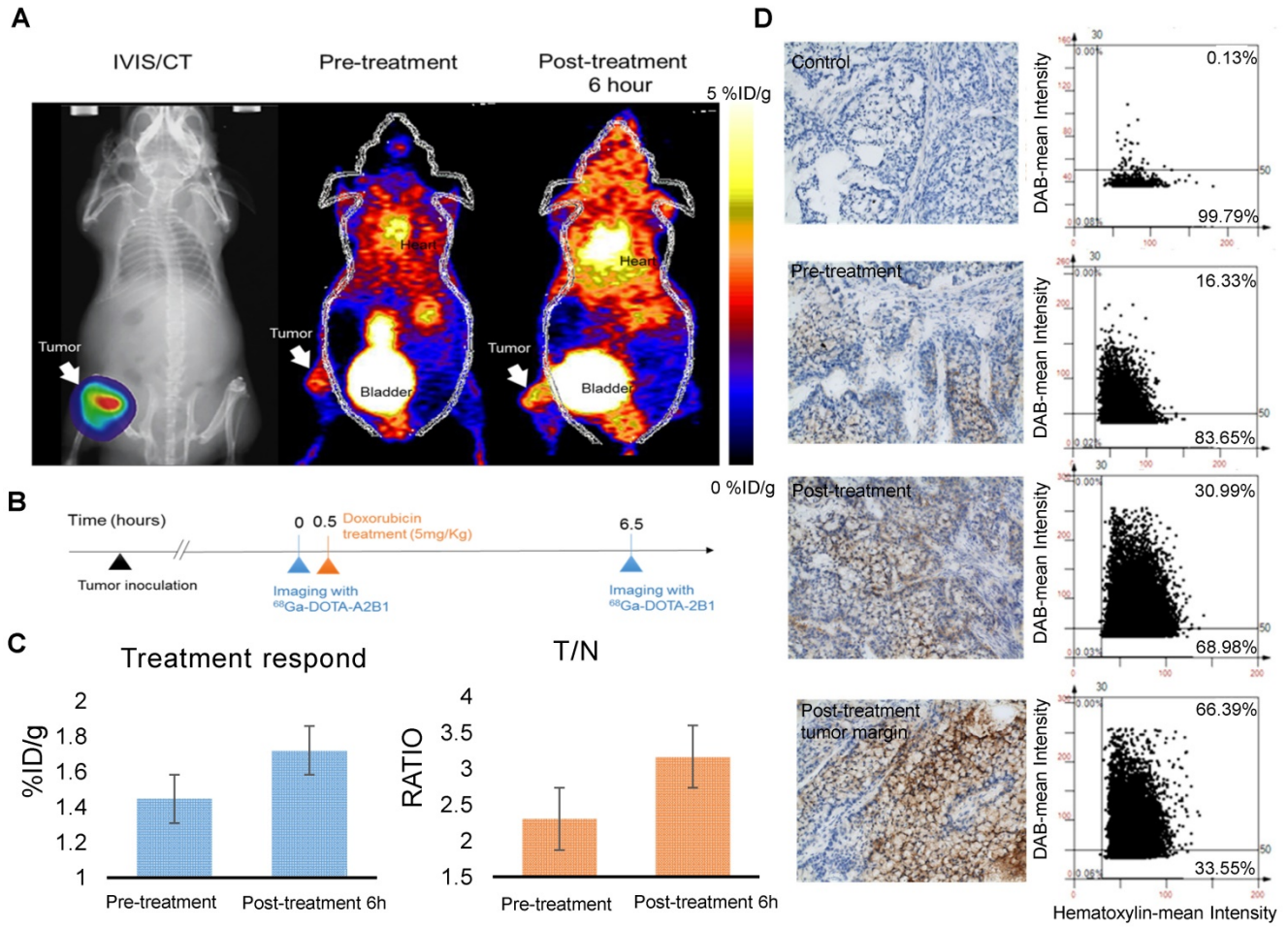

Figure 8. Bone metastasis targeting and treatment response monitoring using ^{68}Ga-DOTA-A2B1 PET imaging *in vivo*. (A) Optical bioluminescence imaging results demonstrated the A549 tumor lesion location, and the PET image clearly shows that ^{68}Ga-DOTA-A2B1 specifically accumulated in osseous tumor grafts located in the left tibia of the mouse, not in the contralateral limb tibia. (B) Schematic representation of the treatment response workflow. Immediately after the first image scan, male mice received a single dose of doxorubicin (5 mg/kg), and at 6 h post-treatment, changes in the drug resistance phenotype were monitored with the ^{68}Ga-DOTA-A2B1 tracer. PET identified a clear region of contrast in the tumor-implanted tibia, where the tracer uptake was significantly higher than in the pretreatment image. (C) Quantitative analysis of ^{68}Ga-DOTA-A2B1 PET tracer uptake. The results indicated significantly elevated (19 %) tumor uptake and an increased T/N ratio, as observed by PET imaging, within 6 h of doxorubicin treatment. *$p < 0.05$. (D) The tumors were collected after the imaging study. The intensity of integrin α2 staining in histological tissue slides was in accordance with the *in vivo* PET imaging results, delineating the up-regulation of integrin expression levels after doxorubicin treatment. In particular, the integrin proteins were intensively stained in the tumor margins.

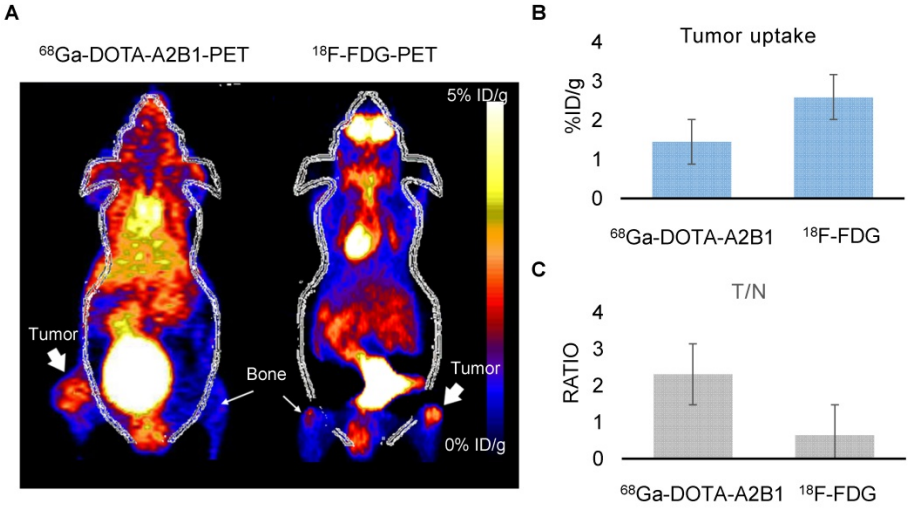

Figure 9. Osseous tumors as evaluated by ^{68}Ga-DOTA-A2B1 and 18F-FDG PET imaging. (A) The animals (n = 4) were sequentially injected with ^{68}Ga-DOTA-A2B1 and ^{18}F-FDG, with one day in between. Clear, high uptake within the tumor lesion was identified for both PET tracers. Although the uptake of ^{18}F-FDG (3.78 ± 0.73 %ID/g) was far greater than that of ^{68}Ga-DOTA-A2B1 (1.58 ± 0.108 %ID/g), the high non-specific uptake of ^{18}F-FDG in the thigh muscle and bone resulted in ambiguous identification of bone metastasis lesions. In contrast, the ^{68}Ga-DOTA-A2B1 PET imaging demonstrated high specific contrast (T/N = 2.31± 0.57) in the tumor region, resulting in a potential advantage over the clinical radiotracer ^{18}F-FDG. (B) Quantification of the data for tumor uptake and the (C) and T/N ratios of both tracers.

In brief, early ^{68}Ga-DOTA-A2B1-PET imaging provided instant visualization for treatment assessment, which may facilitate precision medicine based on individual conditions and make early changes in therapeutic treatment possible. Moreover, this approach could provide the opportunity to monitor the evolving progression of drug resistance, ensuring that PET imaging can be co-registered with other physiological processes measured by other means. Collectively, the current results obtained in preclinical models of metastatic lung tumors and regarding drug resistance should be further validated to define the sensitivity and specificity of this integrin-targeted imaging agent, with the goal of systemic disease control and assessment in patients with metastatic disease.

Discussion

Non-invasive molecular imaging has gained growing interest and recognition among the oncology community for use in interdisciplinary studies. With unparalleled high sensitivity and exquisite specificity, PET is the most recognized imaging modality for investigating tumor stage, phenotypic behaviors and treatment responses in the clinical setting. The glucose analog FDG is the most commonly used radiotracer, and tumor lesions can be characterized in detail based on the glucose metabolism of heterogeneous tumor regions. Increased FDG uptake was thought to be due to the Warburg effect, in which cancer cells prefer to metabolize glucose by aerobic glycolysis because of mitochondrial dysfunction. However, this theory has been challenged, and growing evidence indicates that FDG uptake is significantly higher in hypoxic cancer cells than in non-hypoxic cancer cells [42-45]. Additionally, aerobic glycolysis occurs in tumor-associated fibroblasts, but not in cancer cells, which challenges the accuracy of FDG-PET as a clinical diagnostic tool.

With the emergence of numerous tumor hallmarks proposed by Hanahan and Weinberg [46, 47], a variety of PET imaging tracers have been developed to specifically target or quantitatively evaluate the profile changes of these biomarkers along with the different stages of tumor progression. Among all discovered biomarkers, integrins play a critical role in regulating a variety of inside-out and outside-in signal transduction pathways in cancer cells. The unique expression profiles and activities of integrins are implicated in the fine-tuning of interactions between tumors and their microenvironments, which supports their utility as potential clinically valuable prognostic markers.

Mounting evidence clearly demonstrates the pro-oncogenic role of integrin α2β1, and its aberrant expression might contribute to tumor-induced invasion and metastasis [21, 22, 31, 32]. Little is known about the biological mechanisms underlying the relationship between integrin α2β1 and adhesion receptors on metastatic cells. In this proof-of-concept study, we first determined that integrin α2β1 might serve as a prognostic marker for advanced NSCLC identification based on *in vitro* quantitative Western blot, flow cytometry, and functional migration and invasion assays in several NSCLC cell lines (CL1-0, CL1-5, A549 and selected A549^{++}). These results demonstrated that the expression level of integrin α2β1 was strongly correlated with the tumorigenic and aggressive behaviors of lung cancer cells. In parallel, we evaluated the newly designed integrin α2β1-targeting tracer ^{68}Ga-DOTA-A2B1 and ^{18}F-FDG for their tumor targeting efficacy in subcutaneous, orthotopic and bone metastatic xenograft models *in vivo*. ^{18}F-FDG demonstrated overall higher tumor uptake, but in terms of contrast value (T/N), the A549 tumor lesions were nearly indistinguishable in PET imaging. However, tumor uptake of the ^{68}Ga-DOTA-A2B1 tracer was strongly correlated with tumor expression of integrin α2β1, with a reasonable uptake value, favorable biodistribution profile and superior T/N, making tumor nodules clearly identifiable in imaging. To our surprise, a prompt response to doxorubicin treatment could be quantified by ^{68}Ga-DOTA-A2B1-PET scans after only 6 h of treatment in osseous tumor models. The quantification of *ex vivo* immunostaining results provided numerical values for the relative integrin α2β1 expression level, which was also strongly correlated with elevated tumor uptake of ^{68}Ga-DOTA-A2B1 tracers.

Based on these promising pre-clinical results and to explore the clinical significance of integrin α2β1 in NSCLC tumors, we analyzed the mRNA expression levels of ITGA2 and ITGB1 in several datasets acquired from the Oncomine online microarray database (http://www.oncomine.org). NSCLC tumors include adenocarcinoma (~40% of NSCLC), squamous cell carcinoma (~25-30% of NSCLC), large cell carcinoma (10-15%) and various other subtypes. ITGA2 mRNA expression was up-regulated in clinical NSCLC specimens in ten datasets, being increased by 1.429- to 4.926-fold of its expression in normal tissue specimens (Figure 10 & Table 2). The ten datasets contained 295 specimens from normal lung or tongue, 106 specimens from squamous cell carcinoma and 568 specimens from lung adenocarcinoma.

In the Talbot Lung dataset, ITGA2 and ITGB1 mRNA expression levels in tumor specimens from patients with squamous cell carcinoma were approximately 1.43- and 1.69-fold of those in normal

lung and tongue, respectively (Figure 10 & 11, Table 2). The Talbot Lung dataset comprises 62 specimens, including 28 normal lung specimens and tongue and 34 squamous cell carcinoma specimens. The data-mining analysis indicated that high ITGA2 and ITGB1 expression levels were also correlated with clinical NSCLC development.

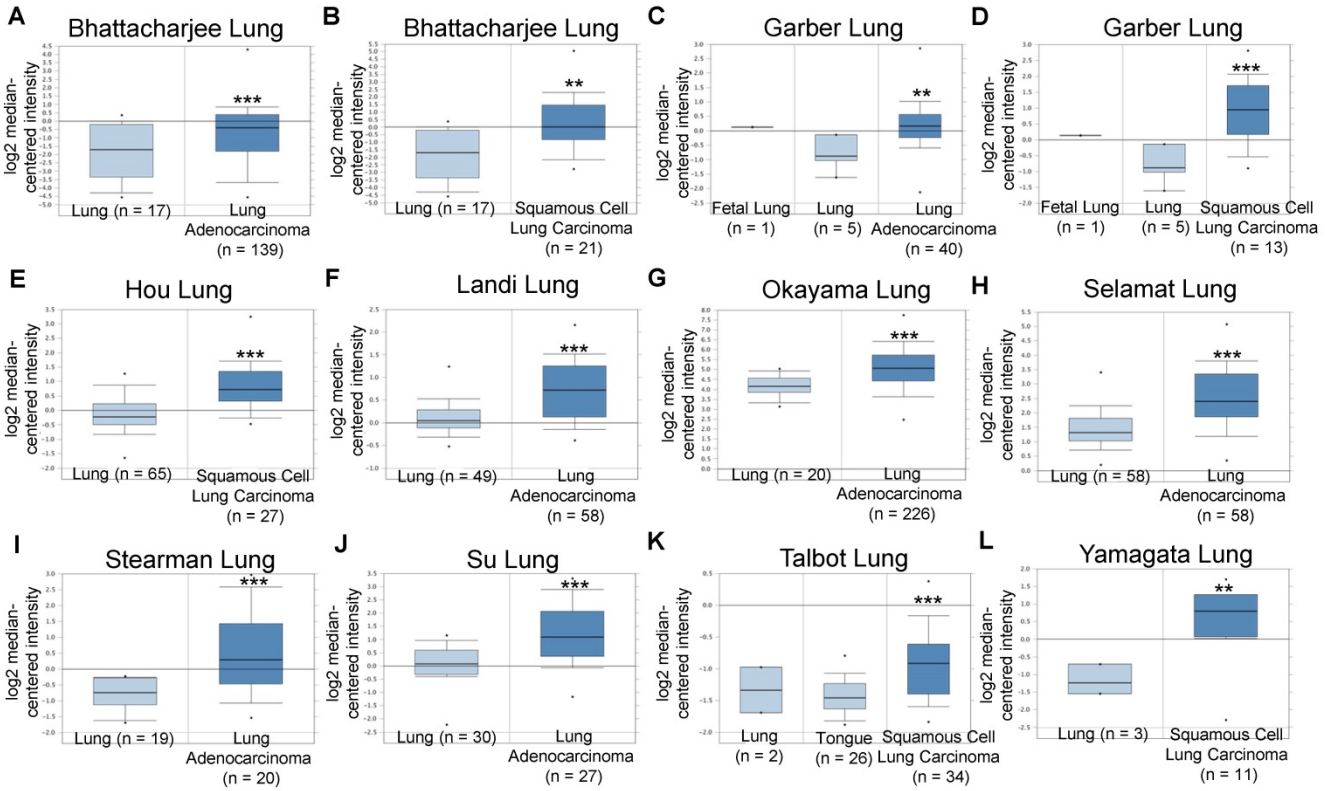

Figure 10. Integrin α2 (ITGA2) expression was up-regulated in NSCLC in clinical cancer samples in ten datasets from the Oncomine online microarray database. The mRNA level of integrin α2 (ITGA2) in clinical NSCLC tumor tissues and normal tissues (lung or tongue) was acquired and analyzed from the Oncomine online microarray database. A box-and-whisker plot that represents ITGA2 expression from primary tumors compared to normal specimens in ten datasets from the Oncomine database. The horizontal top and bottom lines of each box represent the 75th and the 25th percentile, respectively. The band in the box is the median value. Horizontal lines above and below the box represent the 90th and the 10th percentile, respectively. The dots above the 90th percentile and below the 10th percentile represent the maximum and minimum values, respectively. From ten lung datasets, integrin α2 (ITGA2) is up-regulated in tumor tissue specimens in comparison to normal tissues. (A, B) The Bhattacharjee Lung dataset compromises 177 specimens, including 17 normal lung specimens, 21 squamous cell carcinoma specimens and 138 lung adenocarcinoma specimens. (C, D) The Garber Lung dataset compromises 59 specimens, including 6 normal lung specimens, 13 squamous cell carcinoma specimens and 40 lung adenocarcinoma specimens. (E) The Hou Lung dataset comprises 92 specimens, including 65 normal lung specimens and 27 squamous cell carcinoma specimens. (F) The Landi Lung dataset compromises 107 specimens, including 49 normal lung specimens and 58 lung adenocarcinoma specimens. (G) The Okayama Lung dataset compromises 246 specimens, including 20 normal lung specimens and 226 lung adenocarcinoma specimens. (H) The Selamat Lung dataset compromises 116 specimens, including 58 normal lung specimens and 58 lung adenocarcinoma specimens. (I) The Stearman Lung dataset compromises 39 specimens, including 19 normal lung specimens and 20 lung adenocarcinoma specimens. (J) The Su Lung dataset compromises 57 specimens, including 30 normal lung specimens and 27 lung adenocarcinoma specimens. (K) The Talbot Lung dataset comprises 62 specimens, including 28 normal lung and tongue specimens and 34 squamous cell carcinoma specimens. (L) The Yamagata Lung dataset comprises 14 specimens, including 3 normal lung specimens and 11 squamous cell carcinoma specimens. ** $P < 0.01$, *** $P < 0.001$.

Table 2. Integrin α2 (ITGA2) expression was up-regulated in NSCLC in clinical cancer samples from ten datasets

	Dataset	Tumor specimen type (number)	Normal specimen (number)	Gene number	fold change (+)	*p*-value	GEO number
1	Bhattacharjee Lung	Lung adenocarcinoma (139)	Normal Lung (17)	8603	2.315	6.00E-03	-
	Bhattacharjee Lung	Squamous cell lung carcinoma (21)	Normal Lung (17)	8603	4.926	2.08E-04	-
2	Garber Lung	Lung adenocarcinoma (40)	Normal Lung (6)	10945	1.863	7.00E-03	GSE3398
	Garber Lung	Squamous cell lung carcinoma (13)	Normal Lung (6)	10945	2.974	4.91E-04	GSE3398
3	Hou Lung	Squamous cell lung carcinoma (27)	Normal Lung (65)	19574	1.906	1.80E-06	GSE19188
4	Landi Lung	Lung adenocarcinoma (58)	Normal Lung (49)	12624	1.521	5.41E-09	GSE10072
5	Okayama Lung	Lung adenocarcinoma (226)	Normal Lung (20)	19574	1.879	2.13E-07	GSE31210
6	Selamat Lung	Lung adenocarcinoma (58)	Normal Lung (58)	19273	2.155	1.09E-10	GSE32863
7	Stearman Lung	Lung adenocarcinoma (20)	Normal Lung (19)	8603	2.366	2.13E-04	GSE2514
8	Su Lung	Lung adenocarcinoma (27)	Normal Lung (30)	12624	2.253	1.97E-05	GSE7670
9	Talbot Lung	Squamous cell lung carcinoma (34)	Normal Lung (2) Tongue (26)	8603	1.429	1.54E-05	-
10	Yamagata Lung	Squamous cell lung carcinoma (11)	Normal Lung (3)	2509	3.262	1.00E-03	-

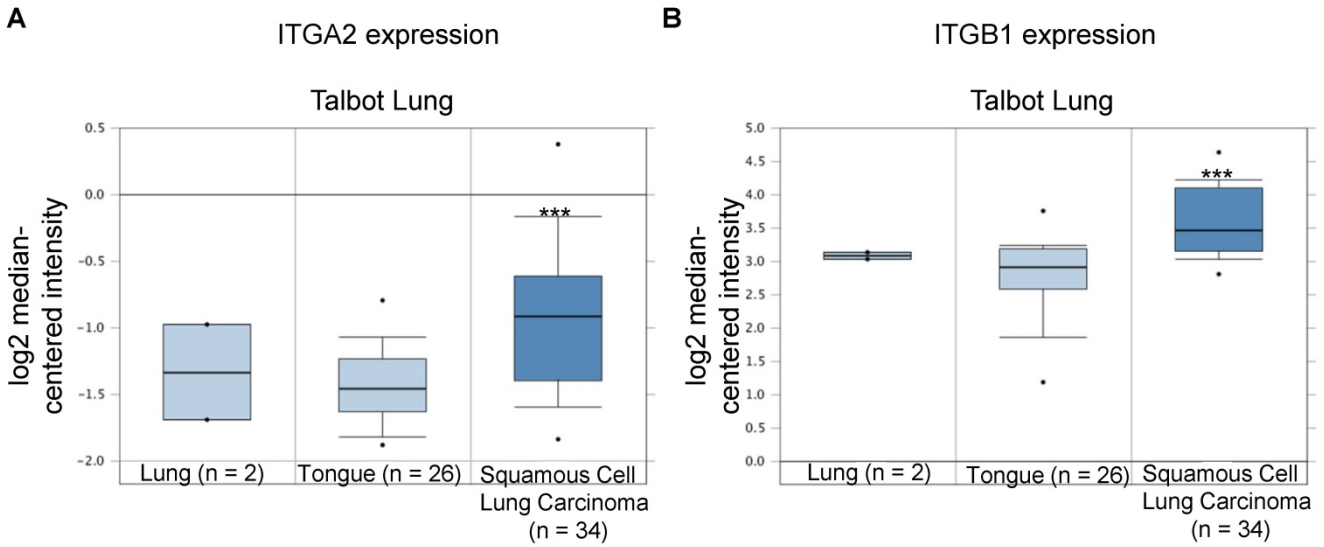

Figure 11. Integrin β1 (ITGB1) expression was upregulated in NSCLC in clinical cancer samples of the Talbot Lung dataset from the Oncomine online microarray database. The Talbot Lung dataset comprises 62 specimens, including 28 normal lung and tongue specimens and 34 squamous cell carcinoma specimens. A box-and-whisker plot that represents ITGB1 expression from primary tumors compared to normal specimens in ten datasets from the Oncomine database. The horizontal top and bottom lines of each box represents the 75th and the 25th percentile, respectively. The band in the box is the median value. Horizontal lines above and below the box represent the 90th and the 10th percentile, respectively. The dots above the 90th percentile and below the 10th percentile represent the maximum and minimum values, respectively. *** $P < 0.001$.

To further understand the biological role of integrin α2β1 in cancer invasion and migration in more depth, the microarray study results of tumor tissues from clinical samples are under further investigation and will extend beyond NSCLC to cover other tumor types, such as breast cancer, prostate cancer and glioma, etc.

Thus, integrin α2β1 may represent an important biomarker for detecting the NSCLC phenotype, and specific integrin α2β1-targeting imaging may improve our understanding of the interactions between cancer cells and their microenvironment, which is a necessary prerequisite for the development of treatment strategies that can specifically target cancer-induced invasion and metastases. This information is significant in light of the correlation of integrin α2β1 over-expression with recurrence and poor prognosis, and it is also valuable for early diagnosis and treatment response monitoring.

Conclusion

The development of agents that can identify integrin α2β1 cell expression profiles, which are considered the "fingerprints" of individual tumors, may have further potential in identifying a cell surface signature for a specific tumor type and/or stage. Based on the results presented in this study, *in vivo* integrin α2β1-targeting molecular imaging will not merely indicate the success or failure of therapy several weeks after initiation, but will play a crucial role in detecting lesions based upon their molecular signatures. Such phenotypic imaging characterization of lesions will aid in translational research of treatment response monitoring and will help define successful therapeutic drug doses on an individual basis.

Abbreviations

PET: Positron emission tomography; NSCLC: non-small cell lung cancer; CT: computed tomography; T/N: tumor-to-normal.

Acknowledgments

The authors thank Dr. Yang Pan-Chyr (National Taiwan University) for kindly providing valuable human non-small cell lung cancer cell lines (CL1-0 and CL1-5).

This work was supported by funds from the Chang Gung Medical Research Program (CMRPG1B0203) and the Ministry of Science and Technology (MOST-105-2314-B-182A-024-).

Supplementary Material

Supplementary figures and tables.
http://www.thno.org/v07p4013s1.pdf

Competing Interests

The authors have declared that no competing interest exists.

References

1. Organization WH. GLOBOCAN 2012: Estimated Cancer Incidence, Mortality and Prevalence Worldwide in 2012. Lung Cancer; 2016.
2. Cancer Genome Atlas Research Network. Comprehensive molecular profiling of lung adenocarcinoma. Nature. 2014; 511: 543–50.

3. Kwak EL, Bang YJ, Camidge DR, Shaw AT, Solomon B, Maki RG, et al. Anaplastic lymphoma kinase inhibition in non-small-cell lung cancer. N Engl J Med. 2010; 363: 1693-703.
4. Bergethon K, Shaw AT, Ou SH, Katayama R, Lovly CM, McDonald NT, et al. ROS1 rearrangements define a unique molecular class of lung cancers. J Clin Oncol. 2012; 30: 863-70.
5. Drilon A, Wang L, Hasanovic A, Suehara Y, Lipson D, Stephens P, et al. Response to Cabozantinib in patients with RET fusion-positive lung adenocarcinomas. Cancer Discov. 2013; 3: 630-5.
6. Kumar M, Ernani V, Owonikoko TK. Biomarkers and targeted systemic therapies in advanced non-small cell lung cancer. Mol Aspects Med. 2015; 45: 55-66.
7. Thomas A, Liu SV, Subramaniam DS, Giaccone G. Refining the treatment of NSCLC according to histological and molecular subtypes. Nat Rev Clin Oncol. 2015; 12: 511-26.
8. Gambhir SS. Molecular imaging of cancer with positron emission tomography. Nat Rev Cancer. 2002; 2: 683-93.
9. Antoch G, Bockisch A. Combined PET/MRI: a new dimension in whole-body oncology imaging? Eur J Nucl Med Mol Imaging. 2009; 36 Suppl 1: S113-20.
10. de Galiza Barbosa F, Delso G, Ter Voert EE, Huellner MW, Herrmann K, Veit-Haibach P. Multi-technique hybrid imaging in PET/CT and PET/MR: what does the future hold? Clin Radiol. 2016; 71: 660-72.
11. Gatenby RA, Gillies RJ. Why do cancers have high aerobic glycolysis? Nat Rev Cancer. 2004; 4: 891-9.
12. Macheda ML, Rogers S, Best JD. Molecular and cellular regulation of glucose transporter (GLUT) proteins in cancer. J Cell Physiol. 2005; 202: 654-62.
13. Vander Heiden MG, Cantley LC, Thompson CB. Understanding the Warburg effect: the metabolic requirements of cell proliferation. Science. 2009; 324: 1029-33.
14. Alavi A, Gupta N, Alberini JL, Hickeson M, Adam LE, Bhargava P, et al. Positron emission tomography imaging in nonmalignant thoracic disorders. Semin Nucl Med. 2002; 32: 293-321.
15. Ben-Haim S, Ell P. 18F-FDG PET and PET/CT in the evaluation of cancer treatment response. J Nucl Med. 2009; 50: 88-99.
16. Doss M, Kolb HC, Zhang JJ, Belanger MJ, Stubbs JB, Stabin MG, et al. Biodistribution and radiation dosimetry of the integrin marker 18F-RGD-K5 determined from whole-body PET/CT in monkeys and humans. J Nucl Med. 2012; 53: 787-95.
17. Wan W, Guo N, Pan D, Yu C, Weng Y, Luo S, et al. First experience of 18F-alfatide in lung cancer patients using a new lyophilized kit for rapid radiofluorination. J Nucl Med. 2013; 54: 691-8.
18. Mi B, Yu C, Pan D, Yang M, Wan W, Niu G, et al. Pilot Prospective Evaluation of (18)F-Alfatide II for Detection of Skeletal Metastases. Theranostics. 2015; 5: 1115-21.
19. Chen H, Niu G, Wu H, Chen X. Clinical Application of Radiolabeled RGD Peptides for PET Imaging of Integrin alphavbeta3. Theranostics. 2016; 6: 78-92.
20. Grzesiak JJ, Bouvet M. The alpha2beta1 integrin mediates the malignant phenotype on type I collagen in pancreatic cancer cell lines. Br J Cancer. 2006; 94: 1311-9.
21. Ibaragi S, Shimo T, Hassan NM, Isowa S, Kurio N, Mandai H, et al. Induction of MMP-13 expression in bone-metastasizing cancer cells by type I collagen through integrin alpha1beta1 and alpha2beta1-p38 MAPK signaling. Anticancer Res. 2011; 31: 1307-13.
22. Grzesiak JJ, Bouvet M. Activation of the alpha2beta1 integrin-mediated malignant phenotype on type I collagen in pancreatic cancer cells by shifts in the concentrations of extracellular Mg2+ and Ca2+. Int J Cancer. 2008; 122: 2199-209.
23. Consonni A, Cipolla L, Guidetti G, Canobbio I, Ciraolo E, Hirsch E, et al. Role and regulation of phosphatidylinositol 3-kinase beta in platelet integrin alpha2beta1 signaling. Blood. 2012; 119: 847-56.
24. Naci D, El Azreq MA, Chetoui N, Lauden L, Sigaux F, Charron D, et al. alpha2beta1 integrin promotes chemoresistance against doxorubicin in cancer cells through extracellular signal-regulated kinase (ERK). J Biol Chem. 2012; 287: 17065-76.
25. Li X, Ishihara S, Yasuda M, Nishioka T, Mizutani T, Ishikawa M, et al. Lung cancer cells that survive ionizing radiation show increased integrin alpha2beta1- and EGFR-dependent invasiveness. PLoS One. 2013; 8: e70905.
26. Staatz WD, Fok KF, Zutter MM, Adams SP, Rodriguez BA, Santoro SA. Identification of a tetrapeptide recognition sequence for the alpha 2 beta 1 integrin in collagen. J Biol Chem. 1991; 266: 7363-7.
27. Huang CW, Li Z, Cai H, Chen K, Shahinian T, Conti PS. Design, synthesis and validation of integrin alpha2beta1-targeted probe for microPET imaging of prostate cancer. Eur J Nucl Med Mol Imaging. 2011; 38: 1313-22.
28. Huang CW, Li Z, Conti PS. In vivo near-infrared fluorescence imaging of integrin alpha2beta1 in prostate cancer with cell-penetrating-peptide-conjugated DGEA probe. J Nucl Med. 2011; 52: 1979-86.
29. Chung YH, Hsu PH, Huang CW, Hsieh WC, Huang FT, Chang WC, et al. Evaluation of prognostic integrin alpha2beta1 PET tracer and concurrent targeting delivery using focused ultrasound for brain glioma detection. Mol Pharm. 2014; 11: 3904-14.
30. Chu YW, Yang PC, Yang SC, Shyu YC, Hendrix MJ, Wu R, et al. Selection of invasive and metastatic subpopulations from a human lung adenocarcinoma cell line. Am J Respir Cell Mol Biol. 1997; 17: 353-60.
31. Matsuoka T, Yashiro M, Nishimura S, Inoue T, Fujihara T, Sawada T, et al. Increased expression of alpha2beta1-integrin in the peritoneal dissemination of human gastric carcinoma. Int J Mol Med. 2000; 5: 21-5.
32. Hall CL, Dai J, van Golen KL, Keller ET, Long MW. Type I collagen receptor (alpha 2 beta 1) signaling promotes the growth of human prostate cancer cells within the bone. Cancer Res. 2006; 66: 8648-54.
33. Hall CL, Dubyk CW, Riesenberger TA, Shein D, Keller ET, van Golen KL. Type I collagen receptor (alpha2beta1) signaling promotes prostate cancer invasion through RhoC GTPase. Neoplasia. 2008; 10: 797-803.
34. Sottnik JL, Daignault-Newton S, Zhang X, Morrissey C, Hussain MH, Keller ET, et al. Integrin alpha2beta 1 (alpha2beta1) promotes prostate cancer skeletal metastasis. Clin Exp Metastasis. 2013; 30: 569-78.
35. Bartolome RA, Barderas R, Torres S, Fernandez-Acenero MJ, Mendes M, Garcia-Foncillas J, et al. Cadherin-17 interacts with alpha2beta1 integrin to regulate cell proliferation and adhesion in colorectal cancer cells causing liver metastasis. Oncogene. 2014; 33: 1658-69.
36. Naci D, Vuori K, Aoudjit F. Alpha2beta1 integrin in cancer development and chemoresistance. Semin Cancer Biol. 2015; 35: 145-53.
37. Sethi T, Rintoul RC, Moore SM, MacKinnon AC, Salter D, Choo C, et al. Extracellular matrix proteins protect small cell lung cancer cells against apoptosis: a mechanism for small cell lung cancer growth and drug resistance in vivo. Nat Med. 1999; 5: 662-8.
38. Rintoul RC, Sethi T. Extracellular matrix regulation of drug resistance in small-cell lung cancer. Clin Sci (Lond). 2002; 102: 417-24.
39. Tsurutani J, West KA, Sayyah J, Gills JJ, Dennis PA. Inhibition of the phosphatidylinositol 3-kinase/Akt/mammalian target of rapamycin pathway but not the MEK/ERK pathway attenuates laminin-mediated small cell lung cancer cellular survival and resistance to imatinib mesylate or chemotherapy. Cancer Res. 2005; 65: 8423-32.
40. El Azreq MA, Naci D, Aoudjit F. Collagen/beta1 integrin signaling up-regulates the ABCC1/MRP-1 transporter in an ERK/MAPK-dependent manner. Mol Biol Cell. 2012; 23: 3473-84.
41. Hodkinson PS, Elliott T, Wong WS, Rintoul RC, Mackinnon AC, Haslett C, et al. ECM overrides DNA damage-induced cell cycle arrest and apoptosis in small-cell lung cancer cells through beta1 integrin-dependent activation of PI3-kinase. Cell Death Differ. 2006; 13: 1776-88.
42. Bensinger SJ, Christofk HR. New aspects of the Warburg effect in cancer cell biology. Semin Cell Dev Biol. 2012; 23: 352-61.
43. Upadhyay M, Samal J, Kandpal M, Singh OV, Vivekanandan P. The Warburg effect: insights from the past decade. Pharmacol Ther. 2013; 137: 318-30.
44. Li XF, Du Y, Ma Y, Postel GC, Civelek AC. (18)F-fluorodeoxyglucose uptake and tumor hypoxia: revisit (18)f-fluorodeoxyglucose in oncology application. Transl Oncol. 2014; 7: 240-7.
45. Zhang G, Li J, Wang X, Ma Y, Yin X, Wang F, et al. The reverse Warburg effect and 18F-FDG uptake in non-small cell lung cancer A549 in mice: a pilot study. J Nucl Med. 2015; 56: 607-12.
46. Hanahan D, Weinberg RA. The hallmarks of cancer. Cell. 2000; 100: 57-70.
47. Hanahan D, Weinberg RA. Hallmarks of cancer: the next generation. Cell. 2011; 144: 646-74.